Available online at www.sciencedirect.com
ScienceDirect
Catalysis Today 120 (2007) 374–382
CATALYSIS TODAY
www.elsevier.com/locate/cattod

Molecular simulation of hydrogen adsorption in organic zeolite

Mee Kyung Song [a,*], Kyoung Tai No [a,b]

[a] *Bioinformatics & Molecular Design Research Center, B138A, Yonsei Engineering Research Complex, Yonsei University, Seoul 120-749, Republic of Korea*
[b] *School of Chemical Engineering and Biotechnology, Yonsei University, Seoul 120-749, Republic of Korea*

Available online 13 November 2006

Abstract

The adsorption of molecular hydrogen on model zeolites has been simulated employing Grand Canonical Monte Carlo (GCMC) procedure. The effects of cation type, available volume, surface area, temperature, pressure and pre-adsorbed organics such as benzene on the hydrogen uptake are analyzed. The hydrogen adsorption can be affected mainly by the available volume and surface area per g-zeolite at the same temperature and pressure. Increase of temperature results in the decrease of sorption intensity and capacity. The adsorption capacity correlates well with the pressure with high linearity at room temperature. Adsorption is lowered by the pre-adsorbed benzene molecule. The orientation and the number of benzene molecule in zeolite affect the adsorption capacity. The organic zeolite with larger available volume shows larger adsorption capacity.

Keywords: Hydrogen adsorption; Organic zeolite; GCMC simulation; Surface area; Available volume

1. Introduction

Since hydrogen has been regarded as a renewable energy carrier, the recent development of microporous metal organic frameworks (MOF), in which metal ions and clusters are linked by organic molecules containing aromatic rings, has initiated intensive research on that material for hydrogen storage [1–6]. MOF can be synthesized in variable structures and functional groups with adjustable pore size, shape and functionality by some adequate combination of metal atoms and organic linker molecules, which leads to the possibility of rational design of sorbents as gas sorption materials. It has been reported that in order to have high volumetric and gravimetric density of adsorbed hydrogen gas, no large voids or mesopores without providing adsorption sites and the light elements in the framework should present in the material, respectively. Furthermore, the faces of aromatic rings of organic linkers are of primary importance in determining hydrogen uptake [7]. Namely, the capacity of hydrogen uptake strongly depends on the electronic feature of organic linkers. However, there is no clear evidence for strict correlation between hydrogen uptake and surface area and pore volume [3,4,8].

Zeolite, naturally occurring aluminosilicates, also has the similar structural frameworks as MOF with open, perfectly regular molecular sized cavities and channels, and can be synthesized in high crystallinity, purity and large amounts with low cost [9]. However, only limited works have been carried out as to the characteristics of hydrogen adsorption in zeolites. The adsorption of gases inside zeolites is the basis of many industrial processes for gas purification and separation [10]. In the crystalline zeolites, the adsorption isotherms do not exhibit hysteresis, so the adsorption and desorption are completely reversible so that the contour of the desorption isotherm follows that of adsorption. Thus, zeolites can be used for hydrogen storage materials when we consider the geometry and the characteristics of adsorption in zeolites. By varying some parameters such as surface area, pore volume, Si/Al ratio, and the content and type of cations, the hydrogen adsorption capacity of zeolites can be controlled [11,12].

Numerical simulations have been used for evaluating the possibility of computing the amount of gas adsorbed at a given temperature and pressure with acceptable precision. Several theoretical studies ranging from force field optimization, molecular dynamics, Monte Carlo simulation, and quantum mechanical calculations have been carried out to identify the characteristics of hydrogen sorption in zeolites and to investigate the possibility of hydrogen storage materials [13–16]. Along with some theoretical studies, the experiments

* Corresponding author. Tel.: +822 393 9550; fax: +822 393 9554.
E-mail address: mksong@bmdrc.org (M.K. Song).

0920-5861/$ – see front matter © 2006 Elsevier B.V. All rights reserved.
doi:10.1016/j.cattod.2006.09.011

for the hydrogen sorption in various zeolites also have been carried out. It has revealed that sodalite could store 0.082 wt.% of hydrogen at about 300 °C and 100 bar [17] and by decreasing temperature, hydrogen uptake values in Na form of faujasite zeolites have been increased to about 1.2 wt.% at −196 °C [12]. Recently, a systematic investigation of hydrogen adsorption in zeolites was carried out [11,18]. It appears that hydrogen uptake in zeolites is strongly dependent on temperature and the type of framework and cation. And also, micropore surface area and micropore volume has a dominat role in the hydrogen adsorption [18].

In this study, the use of zeolite as media for hydrogen storage is investigated. We would like to examine the main factors that affect the hydrogen uptake on several cation-exchanged zeolites by theoretically. The influence of cation type, temperature, pressure and pre-adsorbed organics within the supercage of faujasite on the hydrogen sorption performance is investigated using Grand Canonical Monte Carlo (GCMC) calculations. We may think that there is competitive adsorption between hydrogen and organics. The pre-adsorbed organics lowers the available volume of the zeolite host, where the hydrogen can be adsorbed. However, the organics with π-electron, as aromatic compounds, would increase the interaction with incoming hydrogen, and so may increase the hydrogen adsorption capacity. So, we modeled two simple benzene-adsorbed models with another orientation, and investigated the hydrogen adsorption capacity. All simulations are performed using the Molecular Simulation Inc. (MSI) Cerius^2 simulation package on a SGI Origin300 8-CPU cluster.

2. Computational details

2.1. Construction of zeolite host

The initial model zeolite $Ca_{48}X$ was constructed according to the results of X-ray crystallographic study for dehydrated $Ca_{46}X$ ($X = Si_{100}Al_{92}O_{384}$, Si/Al = 1.1) [19]. The zeolite structure was described in the *Fd*-3 cubic space group with $a = 25.024$ Å and 16 Ca^{2+} ions fill site I and 30 at site II. So, we constructed $Ca_{48}X$ ($X = Si_{96}Al_{96}O_{384}$, Si/Al = 1.0) with 16 Ca atoms at site I and 32 at site II, which are the full atomic numbers per unit cell at each site, and with the same space group.

For the determination of the net atomic charges of Ca and framework atoms Si, Al, and O, the charge equilibration using QEq-charged1.1, implemented in Cerius^2, was applied. After constructing the initial structure and charges, we minimize the structure without any constraint using the conjugate gradient algorithm. The Buchart1.02-Universal1.01 force field [20,21], which was developed to describe the energetics of zeolites–organic molecule system and has been fully validated by MSI, are used. To model the $M_{48}X$ zeolites where M = Mg, Sr, Ba, Mn, and Cd, all Ca atoms of initial structure are substituted with M and the same processes such as charge equilibration and minimization, are applied. These minimized zeolites $M_{48}X$ are used as hosts for hydrogen adsorption. Table 1 shows the minimized $M_{48}X$ structures and the net atomic charges of each atom.

2.2. Force field

For the hydrogen adsorption on zeolite $M_{48}X$, we have used Buchart1.02-Universal1.01 force field [20,21]. The Burchart force field treats the framework and the Universal force field treats the intra- and intermolecular interactions; and the parameters for the framework–molecule interactions are derived from parameters from both force fields, combined by the geometric combination rule. Because the zeolite host has been treated as a rigid structure, with fixed atom positions obtained from the minimized structure, at all simulations, only the non-bond interaction energy is calculated for hydrogen adsorption. The total host–guest interaction energy consists of the sum of a long-range coulombic term and a short-range van der Waals (vdW) term:

$$E_{\text{total}} = E_{\text{el}} + E_{\text{vdW}} \tag{1}$$

$$E_{\text{el}} = \sum_i \sum_{j>i} \frac{q_i q_j}{r_{ij}} \tag{2}$$

where q_i and q_j are the net atomic charges of the ith and jth atoms, respectively, and r_{ij} is the distance between the ith and jth atoms. Since the electrostatic interaction is long-range interaction and the model systems are periodic, Ewald sums are used for E_{el}. The Lennard–Jones (LJ) type potential energy function has been used to describe the vdW interactions as:

$$E_{\text{vdW}} = \sum_i \sum_{j>i} D_{ij} \left\{ -2\left(\frac{\sigma_{ij}}{r_{ij}}\right)^6 + \left(\frac{\sigma_{ij}}{r_{ij}}\right)^{12} \right\} \tag{3}$$

where D_{ij} and σ_{ij} are the LJ potential parameters and r_{ij} is the interatomic distance between the ith and jth atoms. The geometric combination rule is applied for the vdW interaction

Table 1
The minimized structures of $M_{48}X$ ($X = Si_{96}Al_{96}O_{384}$, space group = *Fd*-3) and the net atomic charges, q, for elements of the model systems[a]

Zeolite	E_{min} (10^4 kcal/mol)	Cell length (Å)	q_{Si} (e)	q_{Al} (e)	$q_{\text{O(1)}}$ (e)	$q_{\text{O(2)}}$ (e)	$q_{\text{O(3)}}$ (e)	$q_{\text{O(4)}}$ (e)	$q_{\text{M(I)}}$ (e)	$q_{\text{M(II)}}$ (e)
$Mg_{48}X$	−9.716	25.178	1.244	1.050	−0.619	−0.630	−0.639	−0.607	0.633	0.288
$Ca_{48}X$	−9.700	25.217	1.190	1.003	−0.641	−0.627	−0.630	−0.636	1.026	0.510
$Sr_{48}X$	−9.680	25.233	1.173	0.987	−0.647	−0.620	−0.611	−0.652	1.091	0.566
$Ba_{48}X$	−9.677	25.245	1.158	0.973	−0.652	−0.608	−0.618	−0.659	1.188	0.626
$Mn_{48}X$	−9.712	25.166	1.229	1.038	−0.622	−0.640	−0.639	−0.617	0.678	0.414
$Cd_{48}X$	−9.737	25.169	1.295	1.088	−0.591	−0.614	−0.639	−0.599	0.264	0.047

[a] In zeolite $M_{48}X$, there are four oxygen sites O(1), O(2), O(3), and O(4), and two cation sites, M(I) at site I and M(II) at site II.

Table 2
Lennard–Jones potential energy parameters used for hydrogen adsorption on $M_{48}X$

Atom type[a]	D_0 (kcal/mol)	σ_0 (Å)
Si_z	0.0469	4.2000
Al_z	0.0292	4.2400
O_z	0.1648	3.3000
Mg	0.1110	3.0210
Ca	0.2380	3.3990
Sr	0.2350	3.6410
Ba	0.3640	3.7030
Mn	0.0130	2.9610
Cd	0.2280	2.8480
H	0.0440	2.8860

[a] For $M_{48}X$, four different atom types are considered, three for framework atoms and one for M atom. Si_z, Al_z and O_z represent the Si, Al and O atoms in the zeolite framework, respectively. The Burchart force field treats the framework and the Universal force field treats the intra- and intermolecular interactions; and the parameters for the framework–molecule interactions are derived from parameters from both force fields, combined by the geometric combination rule.

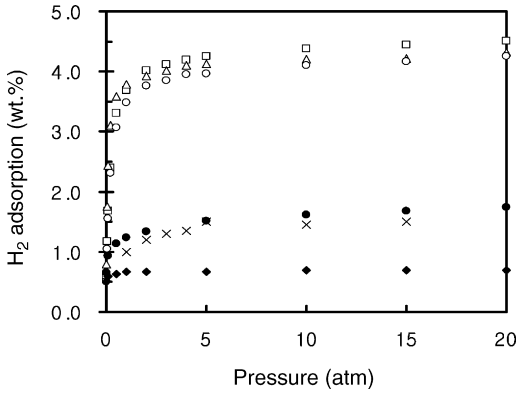

Fig. 1. Simulated adsorption isotherms of H_2 in $Mg_{48}X$ (□), $Ca_{48}X$ (△), $Mn_{48}X$ (○), $Mn_{48}X$–$C_6H_6(p)$ (●) and $Mn_{48}X$–$C_6H_6(l)$ (◆) and the experimental results for MgX (×). All data sets are obtained at 77 K. For $Mn_{48}X$–$C_6H_6(p)$ model, each benzene plane is modeled perpendicularly to each site II Mn cations as in Ref. [24]. Thus, 32 benzene molecules are present in the unit cell of zeolite. For $Mn_{48}X$–$C_6H_6(l)$ model, two Mn cations at site II are linked by one benzene molecule. Thus, total of 48 benzene molecules are present in the unit cell of zeolite (see Fig. 9, for two $Mn_{48}X$–C_6H_6 model structures).

parameters, D_{ij} and σ_{ij}. LJ potential energy parameters used in our calculations are summarized in Table 2.

Darkrim and Levesque (DL) hydrogen potential [22], which treats hydrogen as a rigid diatomic molecule with H–H distance fixed at 0.74 Å was used. This potential represents the experimental value for the quadrupole moment of molecular hydrogen and consists of a LJ core placed at the center of mass of hydrogen molecule, point charges of magnitude $q = 0.483e$ at the two protons' position, and a charge of magnitude $-2q$ at the center of mass.

2.3. Grand Canonical Monte Carlo (GCMC) simulations

Because the GCMC simulations [23] are the most common technique for predicting the zeolite adsorption equilibra, we carried out the GCMC simulations assuming the structure of host zeolite to be rigid during the sorption process. We do not treat the possibility of cation migration, although some redistribution of cations can be occurred by hydrogen adsorption. Only the sorbate hydrogen molecules are placed at random locations inside the zeolite cavity. The metropolis scheme is used at a constant pressure and temperature. Any random molecular configuration is accepted with a probability that decreases exponentially with total energy between the host zeolite and the sorbate molecular hydrogen. The periodic boundary conditions are applied in all three dimensions. All average energies were obtained over 3×10^6 iterations. The cut-off distances of 15 Å for a short-range LJ summation and the half of the cell length for Ewald summation were used. The software of the MSI sorption module was used for all these GCMC simulations.

3. Results and discussion

Cation exchange in zeolites is accompanied by dramatic alteration of stability, adsorption behavior and selectivity, catalytic activity and other important physical properties. Since many of these properties depend upon the controlled cation exchange with particular cation species, detailed information on the cation exchange is important. Although cation exchange may do not go to completion due to the ion-sieve effect, we assumed 100% ion exchange and constructed $M_{48}X$ model. To study the mechanism of hydrogen adsorption in $M_{48}X$, adsorption isotherms of H_2 in $Mg_{48}X$, $Ca_{48}X$ and $Mn_{48}X$ were simulated at 77 K and are shown in Fig. 1. At this temperature, the simulation finds somewhat higher loading than the

Table 3
The available volume, surface area, the hydrogen adsorption capacity and the averaged adsorption energy at 77 K and 15 atm for $M_{48}X$

Zeolite	AV (10^3 Å^3/uc)	AV[a] (Å^3/g)	SA (10^3 Å^2/uc)	SA[a] (Å^2/g)	Adsorption capacity (wt.%)	Adsorption energy (kcal/mol)
$Mg_{48}X$	8.487	0.674	5.416	0.430	4.45	−2.164
$Ca_{48}X$	8.301	0.622	5.471	0.410	4.22	−2.344
$Sr_{48}X$	7.952	0.509	5.351	0.342	3.56	−2.292
$Ba_{48}X$	7.764	0.431	5.234	0.290	3.11	−2.381
$Mn_{48}X$	8.912	0.634	5.687	0.404	4.17	−2.197
$Cd_{48}X$	8.666	0.515	5.692	0.338	3.30	−2.110

[a] AV and SA represent available volume and surface area per g-zeolite, respectively. g-Zeolite represents the molecular weight of the unit cell of model zeolite, $M_{48}X$.

experiment [11] with H_2 loading of about 1.6 wt.% for MgX at 77 K and 15 atm. This suggests that the force field needs to be tuned to get more benefit information. However, in this study, the force field parameter optimization and tuning processes are not carried out, because we would like to figure out the trend and effect of some structural factor of zeolite such as cation type, the atomic net charge, surface area, and the available volume on the hydrogen adsorption.

The influence of ion exchange on hydrogen adsorption was investigated. Simulations of hydrogen adsorption on $M_{48}X$ zeolite are carried out at 77 K and 15 atm along with the calculation of the available volume (AV) and surface area (SA) for the minimized $M_{48}X$. As shown in Table 3, the AV and SA per unit cell of $Sr_{48}X$ and $Ba_{48}X$, both of them have rather large cations Sr and Ba, are smaller than those of the other zeolites. The adsorption capacity does not show any relationship with any of AV and SA per unit cell. However, the adsorption capacity showed much more clear and linear relationship with the AV and SA per g-zeolite (see Fig. 2). g-Zeolite represents the molecular weight of the unit cell of model zeolite, $M_{48}X$. The linear regression of adsorption capacity to SA and AV per g-zeolite gives correlation coefficients $r^2 = 0.9677$ and 0.9554, respectively. Namely, the hydrogen adsorption capacity increases as each of the SA and AV per g-zeolite becomes large. It seems that the cation, which exists in the zeolite cavity with charge, has little effect on the hydrogen uptake in the model zeolite $M_{48}X$ because the environment of cations such as the number and the cation position has been almost similar during simulation. Rather than cation may affect the intensity of hydrogen adsorption. The adsorption experiment on X-type zeolite with different Si:Al ratios in the framework [12] reported that the amount of adsorbed hydrogen and the number of Na ions at sites II and III in the zeolite structure have close relationship. However, the number of the site II cations was same as 32 in all our simulation models, $M_{48}X$. Thus in this environment, the other structural factor such as AV and SA has been the major factor controlling the hydrogen adsorption.

In Fig. 3, the distribution of adsorption energies of H_2 at 77 K and pressures $p = 0.01$, 0.05, 0.1, 0.2, 0.5, and 1 atm for $Mg_{48}X$, $Ca_{48}X$ and $Mn_{48}X$ are shown. Two main peaks are

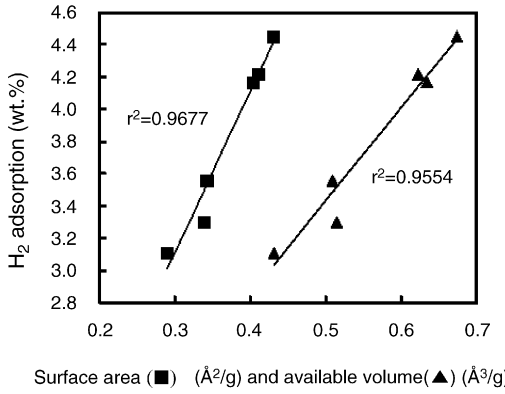

Fig. 2. Linear regression of adsorption capacity for $M_{48}X$ to SA (■) and AV (▲) per g-zeolite. Square represents the value of adsorption capacity vs. SA ($Å^2$/g) and it gives correlation coefficient $r^2 = 0.9677$. Triangle represents the value of adsorption capacity vs. AV ($Å^3$/g) and it gives $r^2 = 0.9554$.

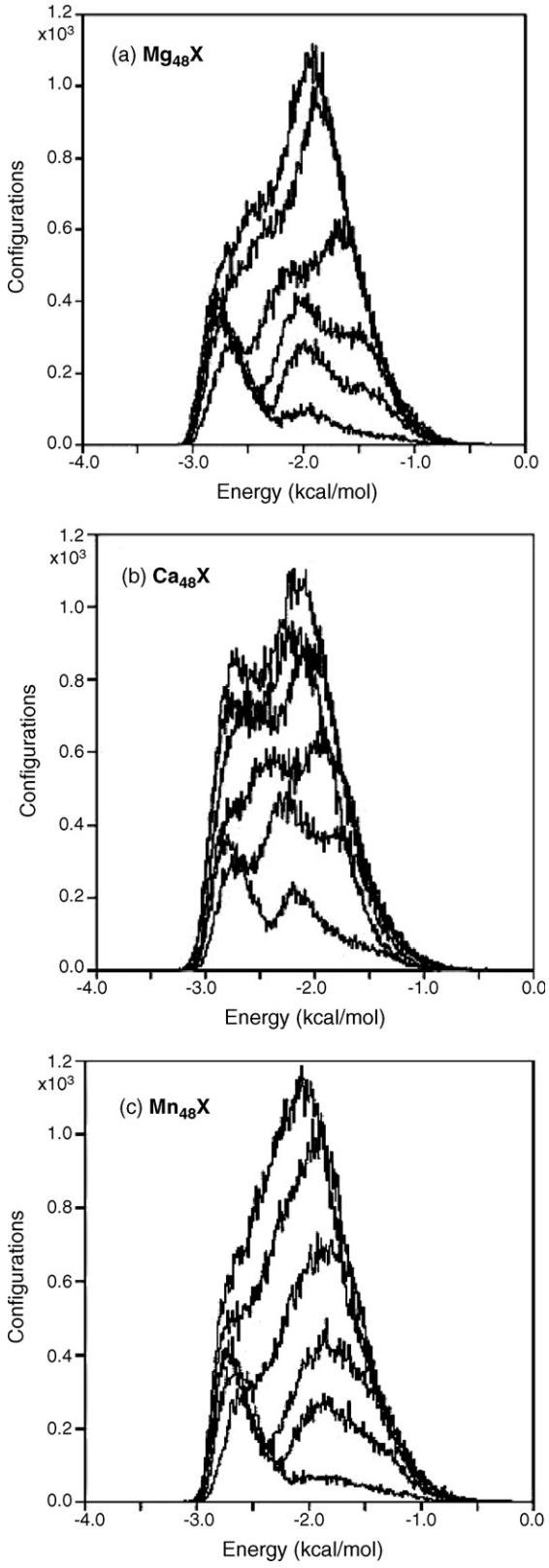

Fig. 3. Distribution of sorption potential energies of H_2 on (a) $Mg_{48}X$, (b) $Ca_{48}X$ and (c) $Mn_{48}X$ at 77 K. From bottom to up, each corresponds to the result at pressure 0.01, 0.05, 0.1, 0.2, 0.5 and 1.0 atm.

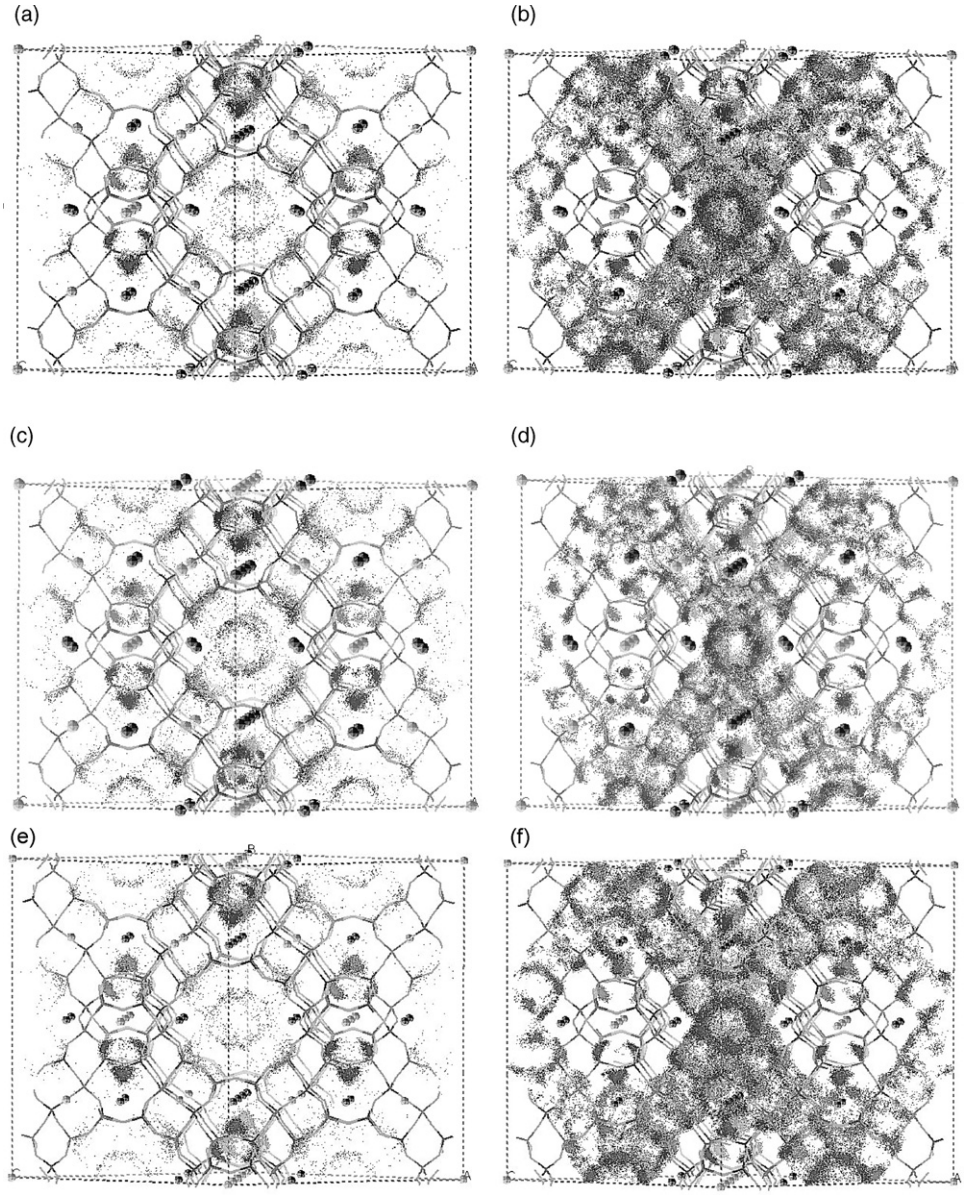

Fig. 4. Mass cloud of H_2 in (a) $Mg_{48}X$ at 0.01 atm, (b) $Mg_{48}X$ at 1 atm, (c) $Ca_{48}X$ at 0.01 atm, (d) $Ca_{48}X$ at 1 atm, (e) $Mn_{48}X$ at 0.01 atm and (f) $Mn_{48}X$ at 1 atm performed at 77 K.

observed for all three systems at 77 K and 0.01 atm. One is centered around −2.8 kcal/mol and the other centered around −2.0 kcal/mol. By increasing the pressure to 0.05 atm, the third peak was observed centered around −1.5 kcal/mol. Since stronger sorption of a molecule results in a more negative value of energy, as shown in the plots, more negative energy values correspond to stronger sorption binding energy. For all three systems, the higher binding energy site was quickly saturated with H_2. This site was distributed homogeneously near the cations in site II and oxygen atoms of zeolite framework. This was confirmed by the observation of the mass density plots as shown in Fig. 4. As the pressure increases, the H_2 molecules cover lower binding energy sites around pre-adsorbed H_2 and the inner pore of zeolite somewhat away from the surface.

In order to figure out the temperature effect on the hydrogen uptake, we carried out simulations at 298 K with pressures up to 100 atm for $Mg_{48}X$, $Ca_{48}X$ and $Mn_{48}X$. As shown in Fig. 5, values of H_2 sorption uptake are almost similar for $Mg_{48}X$ and $Ca_{48}X$ and always higher than those for $Mn_{48}X$. The hydrogen was adsorbed little (∼0.01 wt.%) at room temperature and 1 atm for all zeolites. By increasing the pressure, the adsorption capacity increases to about 0.7 wt.% at 100 atm. The adsorption capacity correlates well with the pressure with $r^2 = 0.9925$, 0.9895 and 0.9920 for $Mg_{48}X$, $Ca_{48}X$ and $Mn_{48}X$, respectively, at 298 K.

The distribution of sorption energies of H_2 at 298 K and $p = 1$, 15, 50 and 100 atm for $Mg_{48}X$, $Ca_{48}X$ and $Mn_{48}X$ are plotted in Fig. 6. At 298 K and 1 atm, it seems that the high binding energy sites become unimportant due to a small density of states and showed a broad range of binding energies from 0 to −3.0 kcal/mol. By increasing pressure, the adsorption of H_2 results in two energetically distinct sorption sites as those at

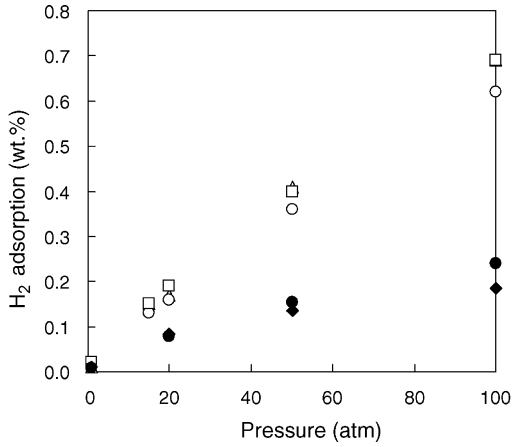

Fig. 5. Simulated adsorption isotherms of H_2 in $M_{48}X$ and $Mn_{48}X$–C_6H_6 at 298 K. Linear regression of hydrogen adsorption capacity for $Mg_{48}X$ (□), $Ca_{48}X$ (△), $Mn_{48}X$ (○), $Mn_{48}X$–$C_6H_6(p)$ (●) and $Mn_{48}X$–$C_6H_6(l)$ (◆) to pressure gives $r^2 = 0.9925$, 0.9895, 0.9920, 0.9769 and 0.9140, respectively.

77 K and the higher binding energy sites are relatively more quickly saturated than the lower binding energy sites. The higher binding energy site was centered around −2.2 kcal/mol and the lower binding energy site was centered around −1.0 kcal/mol. The H_2 molecules are bound weakly to these sorption sites, which were confirmed by the analysis of mass density distribution at 298 K, as shown in Fig. 7. The increased temperature induces H_2 molecules to be distributed more broadly with weak interaction due to the increased kinetic energy. Namely, the adsorption intensity depends much more on the temperature than on the pressure.

In order to see the effect of pre-adsorbed organic molecules on the H_2 adsorption, we built two benzene adsorbed $Mn_{48}X$ models, $Mn_{48}X$–C_6H_6. One is $Mn_{48}X$–$C_6H_6(p)$ model with perpendicular benzene plane to each site II Mn cation. Thus, 32 C_6H_6 molecules are placed in the unit cell of zeolite. According to the experiment [24], benzene adsorbed in zeolite-X like this. The other one is $Mn_{48}X$–$C_6H_6(l)$ model with two Mn ions at site II are linked by one benzene molecule. Thus, there are 6 C_6H_6 molecules per surpercage and 48 C_6H_6 molecules per unit cell of zeolite. The calculated AV and SA for two models are shown in Table 4. By introducing benzene molecule in $Mn_{48}X$ zeolite, the SA, which showed main factor in hydrogen adsorption (see Fig. 2), was increased about one point three times. However, the AV was decreased more than half.

The adsorption of H_2 in $Mn_{48}X$–$C_6H_6(p)$ and $Mn_{48}X$–$C_6H_6(l)$ was simulated at 77 K and the adsorption isotherms are added in Fig. 1. The amount of hydrogen molecules was much small when compared with $Mn_{48}X$ due to the much decreased AV of the zeolite host. In this case, the AV seems to be the key factor for hydrogen adsorption. If SA has increased with large AV decreasing, then the adsorption capacity decreases. This was confirmed by careful investigation of the results represented in Table 4 and Fig. 1. The $Mn_{48}X$–$C_6H_6(p)$, with larger AV and smaller SA than $Mn_{48}X$–$C_6H_6(l)$, has always higher adsorption capacity than $Mn_{48}X$–$C_6H_6(l)$ model. Among the AV and SA, AV gives main effect on the hydrogen adsorption in $Mn_{48}X$–C_6H_6 models.

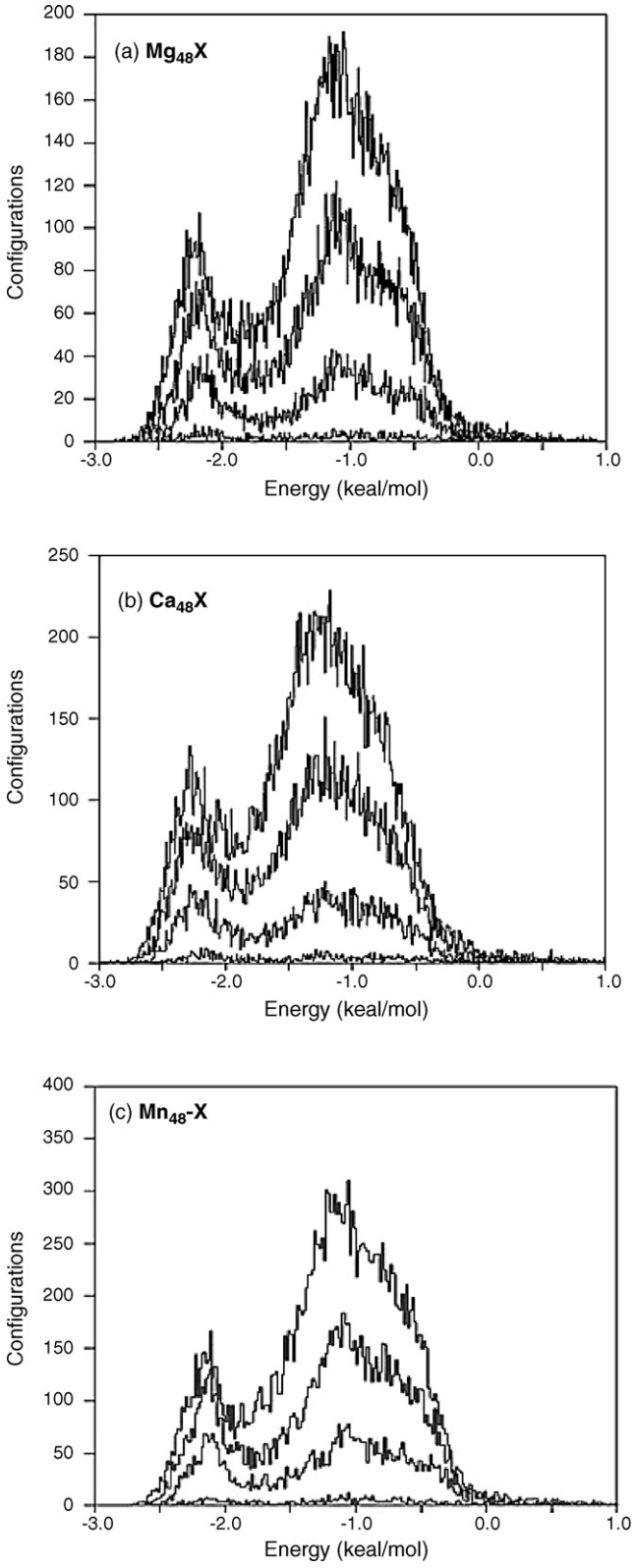

Fig. 6. Distribution of sorption potential energies of H_2 on (a) $Mg_{48}X$, (b) $Ca_{48}X$ and (c) $Mn_{48}X$ at 298 K. From bottom to up, each corresponds to pressure 1, 15, 50, and 100 atm.

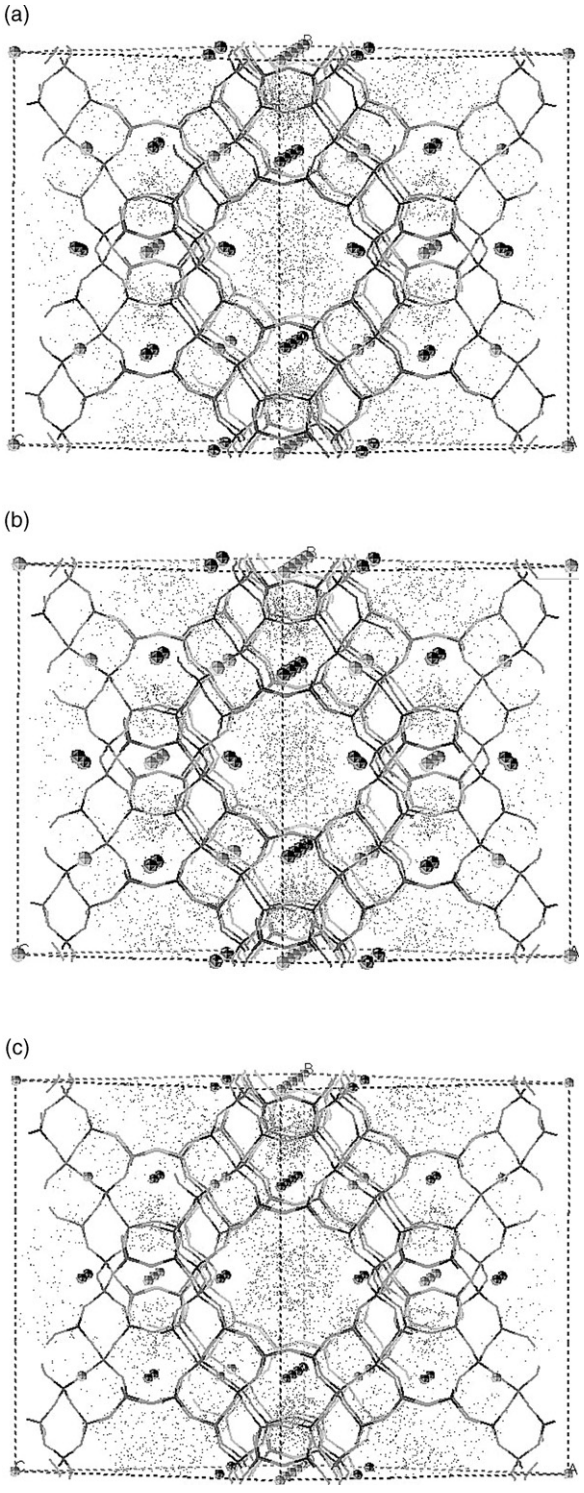

Fig. 7. Mass cloud of H_2 in (a) $Mg_{48}X$, (b) $Ca_{48}X$ and (c) $Mn_{48}X$ at 298 K and 15 atm.

The distribution of adsorption energies of H_2 in $Mn_{48}X$–C_6H_6 models at 77 K and pressures $p = 0.01$, 0.1, 0.5, 1 and 15 atm are shown in Fig. 8(a) and (b). Three adsorption sites are observed at 77 K and 0.01 atm for $Mn_{48}X$–$C_6H_6(p)$. One is centered around −3.5 kcal/mol and the other two centered around −3.0 and −2.3 kcal/mol. By introducing the benzene molecule into the zeolite, the hydrogen adsorption intensity was increased (compare Fig. 8(a) with Fig. 3(c)) because benzene can afford π-electron to the hydrogen and hence increases the interaction with incoming hydrogen. The increase of pressure results in the relative fast saturation of two higher energy sites and the successive incoming H_2 molecules cover lower binding energy sites. In this $Mn_{48}X$–$C_6H_6(p)$ model, the possible adsorption sites are Mn ion, benzene molecule, around pre-adsorbed H_2 and the inner pore of zeolite somewhat away from the surface. The mass density distribution, plot in Fig. 9, confirmed these sites. However, in case of $Mn_{48}X$–$C_6H_6(l)$ model, the link of –Mn–C_6H_6–Mn– makes another inner pore in the supercage of zeolite, which results in the decrease of AV. Hydrogen molecules are adsorbed into this new inner pore with small amount due to the decreased AV and may result in only one broad adsorption site with adsorption energy centered around −3.0 kcal/mol.

The increase of temperature results in the decrease of adsorption capacity, as we have known. The values of H_2 sorption uptake are smaller than $Mn_{48}X$ and almost similar for $Mn_{48}X$–$C_6H_6(p)$ and $Mn_{48}X$–$C_6H_6(p)$ models at 298 K (see Fig. 5). By increasing the pressure, the adsorption capacity increases from 0.01 to about 0.22 wt.% at 100 atm. The adsorption capacity correlates with the pressure with $r^2 = 0.9769$ and 0.9140 for $Mn_{48}X$–$C_6H_6(p)$ and $Mn_{48}X$–$C_6H_6(p)$ models, respectively, at 298 K.

The distribution of adsorption energies of H_2 in $Mn_{48}X$–C_6H_6 models at 298 K and pressures $p = 1$, 15, 50 and 100 atm are also shown in Fig. 8(c) and (d). Three adsorption sites are observed for $Mn_{48}X$–$C_6H_6(p)$. One broad peak was observed between −3.5 and −2.5 kcal/mol and the other two peaks are found centered around −2.3 and −2.0 kcal/mol. For $Mn_{48}X$–$C_6H_6(l)$ model, two adsorption sites are observed; one is centered around −2.8 kcal/mol and the other centered around −2.3 kcal/mol.

From the simulation of benzene-adsorbed zeolites, we could derive that the orientation and the number of benzene, which can make some complex with cations of zeolite, affect the adsorption capacity. Thus, the organic molecules with high affinity for H_2, with no disturbance the interaction of H_2 with host materials, and with no much decrease of AV, can be used for the design of organic zeolites for new hydrogen storage materials.

Table 4
The minimized structure, available volume and surface area for $Mn_{48}X$–$C_6H_6(p)$ and $Mn_{48}X$–$C_6H_6(l)$ (X = $Si_{96}Al_{96}O_{384}$, space group = *Fd*-3) models

Zeolite	E_{min} (10^4 kcal/mol)	Cell length (Å)	AV (10^3 Å^3/uc)	AV[a] (Å^3/g)	SA (10^3 Å^2/uc)	SA[a] (Å^2/g)
$Mn_{48}X$–$C_6H_6(p)$	−9.794	25.126	6.020	0.363	8.635	0.521
$Mn_{48}X$–$C_6H_6(l)$	−9.807	25.119	4.405	0.247	9.902	0.556

[a] AV and SA represent available volume and surface area per g-zeolite, respectively. g-Zeolite represents the molecular weight of the unit cell of model zeolite, $M_{48}X$–C_6H_6.

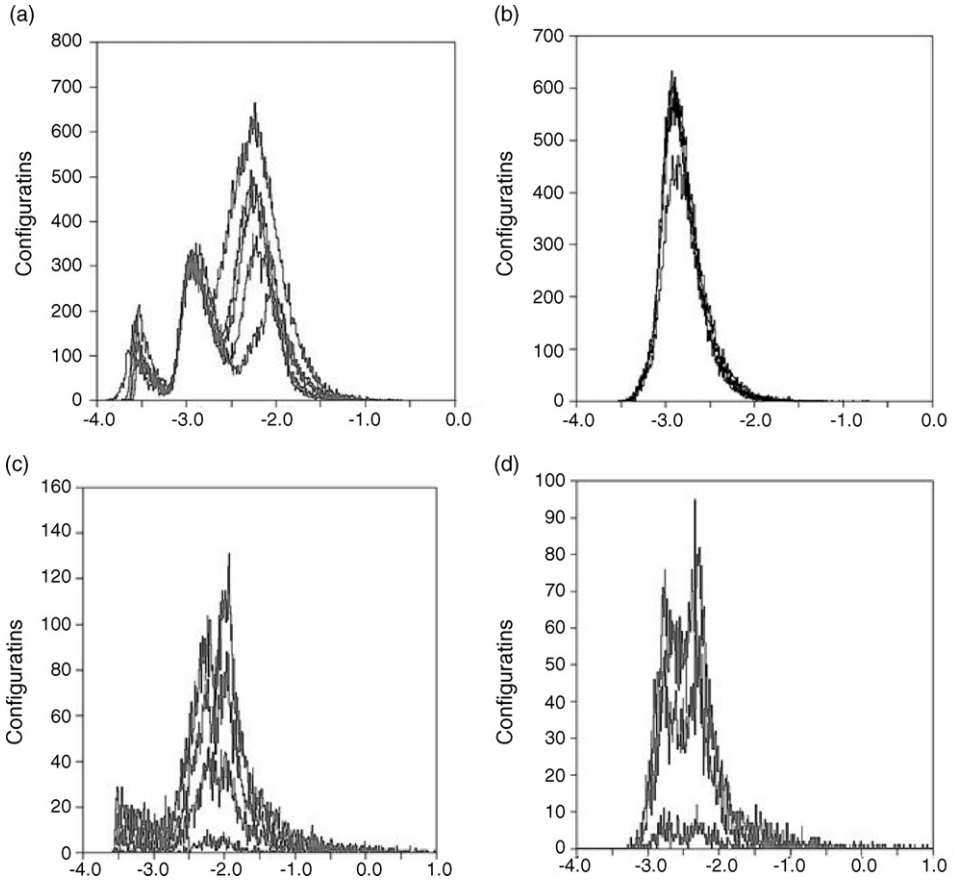

Fig. 8. Distribution of sorption potential energies of H_2 on (a) $Mn_{48}X–C_6H_6(p)$ and (b) $Mn_{48}X–C_6H_6(l)$ at 77 K. From bottom to up each corresponds to pressure 0.01, 0.1, 0.5, 1 and 15 atm. Distribution of sorption potential energies of H_2 on (c) $Mn_{48}X–C_6H_6(p)$ and (d) $Mn_{48}X–C_6H_6(l)$ at 298 K. From bottom to up each corresponds to pressure 1, 20, 50 and 100 atm.

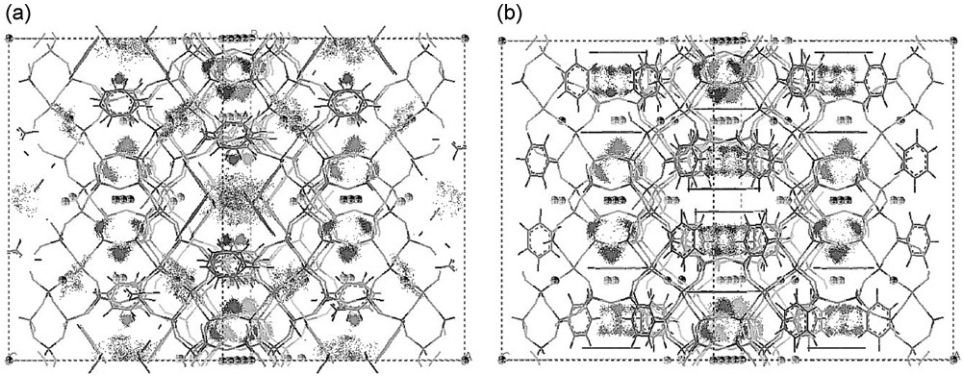

Fig. 9. Mass cloud of H_2 in (a) $Mn_{48}X–C_6H_6(p)$ and (b) $Mn_{48}X–C_6H_6(l)$ at 77 K and 0.01 atm.

4. Conclusions

The numerous adsorption isotherms, which have been obtained by GCMC simulations at 77 K and 298 K, reveals that the hydrogen adsorption is affected mainly by the AV and SA per g-zeolite of host materials at the same temperature and pressure. Not only the adsorption temperature and pressure, but also the pre-adsorbed benzene influences the hydrogen adsorption. Increase of temperature, which induces the increase of thermal energy of hydrogen, results in the decrease of adsorption intensity and capacity. The adsorption capacity correlates well with the pressure with high linearity at 298 K. The pre-adsorbed benzene decreases the hydrogen adsorption due to the decreased AV, although it increases the SA of the zeolite host, and increases the adsorption intensity. The orientation and the number of benzene, which can make some complex with cations of zeolite, affect the adsorption capacity. From the careful investigation of the simulation results, we may conclude that GCMC simulation can be a useful tool for probing the some features of zeolite, such as the

adsorption sites and energy, and design of new hydrogen storage materials.

Acknowledgement

Authors thank to the support for this research from the Hydrogen Energy R&D Center, one of the 21st Century Frontier R&D Program, funded by the Ministry of Science and Technology of Korea.

References

[1] N.L. Rosi, J. Eckert, M. Eddaoudi, D.T. Vodak, J. Kim, M. O'Keeff, O.M. Yaghi, Science 300 (2003) 1127.
[2] X. Zhao, B. Xiao, A.J. Fletche, K.M. Thomas, D. Bradshaw, J. Rosseinsky, Science 306 (2004) 1012.
[3] L. Pan, M.B. Sander, X. Huang, J. Li, M. Smith, E. Bittner, B. Bockrath, J.K. Johnson, J. Am. Chem. Soc. 126 (2004) 1308.
[4] J.L.C. Rowsell, A.R. Millward, K.S. Park, O.M. Yaghi, J. Am. Chem. Soc. 126 (2004) 5666.
[5] S. Kitagawa, R. Kitaura, S.-I. Noro, Angew. Chem. Intl. Ed. 43 (2004) 2334.
[6] E. Sagara, J. Klassen, E. Ganz, J. Chem. Phys. 121 (2004) 12543.
[7] Y.S. Nechaev, O.K. Alexeeva, Int. J. Hydr. Energy 28 (2003) 1433.
[8] D.N. Dybtsev, H. Chun, S.H. Yoon, D. Kim, K. Kim, J. Am. Chem. Soc. 126 (2004) 32.
[9] D.W. Breck, Zeolite Molecular Sieves: Structure, Chemistry and Use, Wiley, New York, 1974.
[10] R.T. Yang, Gas Separation by Adsorption Processes, Imperial College Press, London, 1997.
[11] H.W. Langmi, A. Walton, M.M. Al-Mamouri, S.R. Johnson, D. Book, J.D. Speight, P.P. Edwards, I. Gameson, P.A. Anderson, I.R. Harris, J. Alloy. Compd. 356 (2003) 710.
[12] V.B. Kazansky, V.Y. Borovkov, A. Serich, H.G. Karge, Micropor. Mesopor. Mater. 22 (1998) 251.
[13] C. Anderson, D.F. Coker, J. Eckert, A.L.R. Bug, J. Chem. Phys. 111 (1999) 7599.
[14] F. Darkrim, A. Aoufi, P. Malbrunot, D. Levesque, J. Chem. Phys. 112 (2000) 5991.
[15] E.D. Akten, R. Siriwardane, D.S. Sholl, Energy Fuels 17 (2003) 977.
[16] X. Solans-Monfort, V. Branchadell, M. Sodupe, C.M. Zicovich-Wilson, E. Gribov, G. Spoto, C. Busco, P. Ugliengo, J. Phys. Chem. B 108 (2004) 8278.
[17] J. Weitkamp, M. Fritz, S. Ernst, Int. J. Hydr. Energy 20 (1995) 967.
[18] S.H. Jhung, J.W. Yoon, H. Kim, J. Chang, Bull. Korean Chem. Soc. 26 (2005) 1075.
[19] Y.H. Yeom, S.B. Jang, Y. Kim, S.H. Song, K. Seff, J. Phys. Chem. B 101 (1997) 6914.
[20] E. de V. Burchart, PhD Thesis, 1992. Studies on Zeolites: Moleular Mechanics, Framework Stability and Crystal Growth, Table I, Chapter XII.
[21] A.K. Rappe, C.J. Casewit, K.S. Colwell, W.A. Goddard III, W.M. Skiff, J. Am. Chem. Soc. 114 (1992) 10024.
[22] F. Dakrim, D. Levesque, J. Chem. Phys. 109 (1998) 4981.
[23] M. Allen, D. Tildesley, Computer Simulation of Liquids, Oxford University Press, Oxford, UK, 1981.
[24] Y.H. Yeom, A.N. Kim, Y. Kim, S.H. Song, K. Seff, J. Phys. Chem. B 102 (1998) 6071.